Journal of Applied Fluid Mechanics, Vol. 18, No. 5, pp. 1130-1139, 2025.
Available online at www.jafmonline.net, ISSN 1735-3572, EISSN 1735-3645.
https://doi.org/10.47176/jafm.18.5.3059

Aerodynamic Drag Analysis of Superpressure and Zero Pressure Balloons using Large Eddy Simulations (LES)

B. Lohani[1†] and C. Mascarenhas[2]

[1] *Department of Mechanical Engineering and Materials Science, University of Pittsburgh, Pittsburgh, PA 15261, USA*
[2] *School of Engineering and Applied Sciences, Harvard University, 12 Oxford Street, Cambridge, 02138, USA*

†*Corresponding Author Email: bil56@pitt.edu*

ABSTRACT

Stratospheric balloons are an essential part of the scientific research community. In previous stratospheric balloon models used for trajectory prediction and station-keeping, the aerodynamic drag has usually been modeled as similar to that of a sphere. However, with recent proposals to use propulsion systems on the payload of stratospheric balloons to achieve trajectory control in the horizontal plane, it is important to refine our understanding of the drag of stratospheric balloons, especially at low horizontal velocities near transition, where spherical assumptions may deviate significantly. This study conducts a Computational Fluid Dynamics (CFD) investigation into the aerodynamic characteristics of both superpressure balloons (SPBs) and zero pressure balloons (ZPBs) using Large Eddy Simulations (LES). The analysis was conducted over a range of Reynolds numbers that correspond to reasonable forward airspeeds for horizontal stratospheric propulsion-based balloon systems. The results show that both balloons have drag characteristics qualitatively similar to a sphere. This includes an initially high drag coefficient, a drag crisis, and a lower eventual drag coefficient. Quantitatively, however, differences emerge between the balloon aerodynamics and that of a sphere. For example, the drag crisis occurs at a lower Reynolds number for both types of balloons when compared to a sphere. This is critical as proposed propulsion-based balloon systems aim to operate near the Reynolds number where this drag crisis occurs. The drag coefficient for the SPB was found to be less than the ZPB at all Reynolds numbers. A sensitivity analysis revealed that increasing the number of gores decreased the drag coefficient, with the flow separation delayed and the wake narrowing as the gore count increased. For example, a reduction of 32% in drag was observed when the number of gores increased from 30 to 50.

Article History

Received August 12, 2024
Revised December 8, 2024
Accepted December 22, 2024
Available online March 4, 2025

Keywords:

Large eddy simulation
Superpressure balloon
Zero pressure balloon
Drag coefficient
Stratospheric propulsion
Aerodynamics

1. INTRODUCTION

Stratospheric balloons employed for scientific purposes are a common lighter-than-air vehicle used in science and engineering for data collection and near-space testing of instrumentation. These balloons typically reach float altitudes well into the Earth's stratosphere, often between 18 – 35 km, and are usually equipped with a gondola system that is equipped with payloads comprising of remote sensing devices, cameras, and other instrumentation for weather predictions, atmospheric sampling, space-facing observations, Earth-facing remote sensing, and defense applications (Smith, 2002; Miller et al., 2005; Li et al., 2018).

The balloons are generally either in the form of a superpressure balloon (SPB) or a zero-pressure balloon (ZPB). SPBs are sealed and maintain a positive internal pressure, whereas ZPBs have open ducts and no internal pressure relative to the background environment. SPBs allow for flight times on the order of weeks or months, while ZPB flights usually last for days. The two types of balloons have different use cases, but importantly, they both offer some advantages over satellites for atmospheric data collection, due to the *in-situ* nature of the measurements, lack of ionospheric interference, time spent over the sampling target, relative cost, and high spatial and temporal resolution.

In many applications, the flight profile and trajectory of the balloon are of paramount importance. Due to their

NOMENCLATURE

SPB	Super Pressure Balloon	τ_{sgs}	subgrid stress tensor
ZPB	Zero Pressure Balloon	ν_{sgs}	turbulent viscosity
CFD	Computational Fluid Dynamics	b_d	buoyancy at float
LES	Large Eddy Simulation	V_d	volume of the balloon
EHD	Electro-Hydrodynamic	w_d	weight density of the balloon
ACHAB	Analysis Code for High Altitude Balloon	σ_m	meridian stress
RANS	Reynolds-Averaged Navier Stokes	κ	turbulent kinetic energy
PISO	Pressure Implicit with Splitting of Operators	ϵ	dissipation rate of κ
Open FOAM	Open Field Operation and Manipulation	ω	specific dissipation rate of κ
N	number of gores	C_d	coefficient of drag
d	sphere diameter	F_d	drag force
ρ	fluid density		

widespread use in such applications, various computational programs have been developed in order to predict and assess the flight and trajectory of these balloons (Musso et al., 2004; Sóbester et al., 2014; Saleh & He, 2017; Jewtoukoff et al., 2016). Some of the most commonly used are NASA's Scientific Balloon Analysis Model (SINBAD), as well as Balloon Ascent, which includes the ability to differentiate between SPBs and ZPBs (Garde, 2005; Raque & Robbins; Farley, 2005). Recently, the Italian Aerospace Research Center (CIRA) developed a novel program called Analysis Code for High Altitude Balloons (ACHAB) that features ballasting, valving, and further modeling of stratospheric balloon paths, that achieved good correlation with experimental results (Palumbo et al., 2007).

In order to achieve persistent monitoring over a particular target for an observation mission, the balloon's ability to linger within a certain region is of great importance. This is known as station-keeping and is primarily achieved by leveraging different wind directions and velocities available at different flight altitudes (Fesen & Brown, 2015; Du et al., 2019b; Liu et al., 2022). Various other station-keeping concepts have been developed such as using a wing, a sail, and even electro-hydrodynamic (EHD) thrusters to combat winds (Aaron et al., 2002; van Wynsberghe & Turak, 2016; Ramesh et al., 2018). For all station-keeping and trajectory control of the balloons, however, the aerodynamic drag properties of the balloon affect the simulations and the results.

A stratospheric balloon using a propulsion system for horizontal maneuvering was proposed for the first time for use in a stratospheric aerosol experiment (Dykema et al., 2014). This project originally proposed to use an SPB at 20,000 m to achieve horizontal maneuverability at a local velocity up to 8 m/s, not for station-keeping, but rather for experimental purposes of plume formation within a Lagrangian reference frame. That is, while the background stratospheric winds may carry the system to a different horizontal location over-the-ground (Eulerian reference frame), the scientific experiment was interested in the point-of-view of the plume from the gondola system. Thus, the drag properties of the balloon at the locally-imposed (propeller-based) velocities were of determined to be of critical importance. Later versions of this project proposed experimentation using a ZPB at velocities between 0.5 m/s to 3 m/s. Similarly, Google Loon experimented with propulsion for their stratospheric balloons, and there are other studies investigating horizontal propulsion on stratospheric balloons (Kahyan, 2020).

Due to this potential for propulsion-based control on all types of stratospheric balloons, it is extremely important to understand the aerodynamic properties of both SPBs and ZPBs at their float altitude and shape, as it relates directly to the engineering design of the propulsion system, science related to experimentation in the Lagrangian perspective, and understanding of system-level impact.

In most of the trajectory prediction tools in the literature, the balloon is modeled as a sphere with spherical aerodynamic properties (Dai et al., 2012; Du et al., 2019a; Tang et al., 2022). Often, depending on the Reynolds number, a fixed drag coefficient is used in the model (Musso et al., 2004; Dai et al., 2012). In some cases, drag coefficients based on empirical spherical data are used over a range of Reynolds numbers coupled with tools such as ACHAB and SINBAD (Tang et al., 2022). In the case of the station-keeping concepts as well, spherical approximations for the balloon were used (Ramesh et al., 2018). For the case of horizontal propulsion at low velocities, balloon drag in the forward direction becomes especially important. The unique shape of the balloon may lead to differences in the drag properties when compared to a sphere, and thus is of vital importance in the case of horizontal propulsion, especially at the low Reynolds numbers expected. While spherical modeling may be acceptable at higher Re, the potential deviation in behavior at low Re region around the drag crisis requires investigation, particularly when the drag coefficient is so important.

Studies regarding the aerodynamic drag properties of stratospheric balloons have been scarce. There have been a couple of previous studies using Computational Fluid Dynamics (CFD) to study the drag properties of stratospheric balloons (Sun et al., 2015; Tian et al., 2023). Those studies conducted Reynolds-averaged Navier Stokes (RANS) simulations to understand the drag force on SPBs. Recognizing that RANS-based models, including k-epsilon (k-ε) and k-omega (k-ω), are popular

due to their computational efficiency and capacity to predict time-averaged turbulence features, it is also equally essential to comprehend their limitations in that they sometimes have trouble in representing unfavorable pressure gradients and flow separation (Akhlaghi et al., 2023; Ghafoorian et al., 2024). Sun (2015) also stated that for a more accurate analysis of the performance, a Large Eddy Simulation (LES) should be conducted, which is what our analysis aims to do. Additionally, our study also aims to analyze ZPBs, which have different shapes and thus will have different aerodynamic properties. Furthermore, our study is motivated by the potential for balloons to be propelled in the horizontal plane at low velocities without changing their float altitude, as opposed to simply studying the effects of passive wind shear faced by balloon systems.

2. RESEARCH NEEDS AND OBJECTIVES

With the dawn of propulsion-based horizontal control for stratospheric balloons such as those proposed by Dykema and others, understanding the drag properties of the balloon system is essential, especially at very low velocities. This is because the thrust output required by the propulsion system at a given velocity directly corresponds to the drag force of the system at that velocity, and the balloon drag would be the dominant component of the drag force. As payloads from both SPBs and ZPBs can be equipped with a propulsion system, it is important to study the aerodynamic properties of both balloons so that the propulsion system can be properly sized based on the required forward airspeed. Since the focus of this study is on propulsion-equipped balloon systems capable of low horizontal airspeeds, the goal will be to analyze the drag performance of SPBs and ZPBs at a range of Reynolds numbers that correspond to these low flight velocities in the stratosphere, which end up being between 5E4 and 6E5.

The study will also analyze the effect of the number of balloon gores on drag. This will allow experimenters that are concerned about balloon drag to work with balloon designers to understand whether optimization in the manufacturing domain is possible. However, it is beyond the scope of this analysis to incorporate manufacturing techniques in the analysis or to provide an opinion on the feasibility of the number of gores used.

The results of the study hope to inform researchers about the drag performance of balloons at a variety of different conditions. This will allow for better propulsion system design and optimized flight concept of operations based on the sensitivity of the system drag to airspeed. Additionally, trajectory models and station-keeping programs can refine the aerodynamic drag inputs of the balloons in their models. This study aims to conduct the first LES analysis of stratospheric balloons.

3. MATERIALS AND METHODS

3.1 Governing Equations

Large Eddy Simulations (LES) are a precise family of techniques in CFD that can resolve the majority of the flow's eddy structures. By applying filtering techniques or sub-grid scale modeling, LES resolves eddies that are larger than the grid size and models micro eddies (Moin & Kim, 1982; Givi, 1989; Lesieur & Metais, 1996; Lohani et al., 2022). Only eddies with a Kolmogorov length scale or smaller can be eliminated by the viscous stress tensor. As a result, the dissipation is increased by adding the additional stress term τ_{sgs}, also known as sub-grid stress. An eddy viscosity model that is described in (1) is used to determine τ_{sgs}.

$$\tau_{sgs} = 2\rho\nu_{sgs}S_{ij}^{*} - \frac{2}{3}\rho k_{sgs}\delta_{ij} \tag{1}$$

The resolved eddies on the mesh's strain rate, S_{ij}^{*} are affected by the velocity gradient. Eddies that are larger than the size of the mesh's cells can be dispersed by the tension. The power of τ_{sgs}, which only accounts for the eddy's size and not its shape, is ν_{sgs}. The equation (2) can be used to create a number of sub-grid models that employ various approaches to solve for ν_{sgs}.

$$\nu_{sgs} = \left(C_k\overline{\Delta}\right)^2\sqrt{k_{sgs}} \tag{2}$$

According to the definition of the equation (3), kinetic energy at the sub-grid scale can be transmitted.

$$\frac{\partial k_{sgs}}{\partial t} + \overline{u_i}\frac{\partial k_{sgs}}{\partial x_i} = -\tau_{ij}\frac{\partial \overline{u_i}}{\partial x_j} - C_c\frac{k_{sgs}^{1.5}}{\overline{\Delta}} + \frac{\partial}{\partial x_i}\left(\frac{\nu_{sgs}}{\sigma_k}\frac{\partial k_{sgs}}{\partial x_i}\right) \tag{1}$$

To ensure accuracy in the LES model implemented in OpenFOAM, the WALE sub-grid model was employed due to its effectiveness in capturing near-wall eddy behavior. Constants with standard values of 0.05, 1.0, and 1.0 correspondingly are C_k, C_c and σ_k (Menon et al., 1996).

3.2 Geometry and Boundary Conditions

While the Reynolds number approach allows for non-dimensional fluid dynamics characterization of the system, the actual underlying parameters used in the non-dimensionalizing calculation are driven by typical system values in stratospheric balloon missions. For example, the proposed propulsion-based stratospheric balloon experiment is to be conducted at around 20,000 m, thus the altitude for the ensuing simulations in this study is set as such, with a density of 0.089 kg/m^3 and kinematic viscosity of $1.61E-4\ m^2s^{-2}$. The velocity was varied to correspond to the Reynolds number range under investigation while holding other parameters constant. The fluid was assumed to be incompressible and Newtonian, as density variations are negligible at the low Mach numbers being studied. The balloon size is also driven by the experimental values that require a 600kg payload (L), necessitating a certain balloon size, system mass, and volume, which affect the geometry and characteristic Reynolds length scale of the system as presented in Table 1. The same general requirements are applied to both the ZPB and the SPB in this study for the sake of easier comparison.

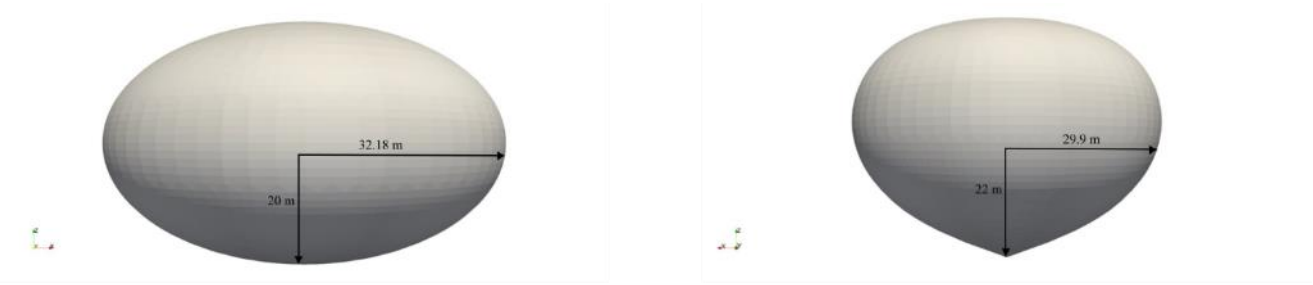

(a) SPB (b) ZPB

Fig. 1 Stratospheric balloons

Table 1 Geometry of the stratospheric balloon

	Volume(m^3)	**Ref. Area** (m^2)	**Ref. Length** (m)
SPB	10,466.95	487.79	32.18
ZPB	10,492.72	525.18	29.9

The shape at the float altitude (i.e. equilibrium) of the SPB and ZPB is characterized by the Archimedes principle. The gross weight of the balloon is balanced by the buoyancy at float (b_d), times the volume (V_d) that is displaced by the balloon. The lift force required for the balloon to cruise at this flight altitude is 7840 N. The specific buoyancy of the balloon as a result of the pressure difference of air and Helium gas at float altitude is 0.751 N/m^3. The shape of an SPB at float altitude can be well approximated with that of an oblate spheroid (Schur, 2002; Cathey Jr, 2009; Sun et al., 2015). The equation 4 represents the mathematical representation of the required shape for the SPB.

$$\frac{x^2+y^2}{a^2}+\frac{z^2}{b^2}=0 \tag{2}$$

where a is the length of the equatorial radius and b is the polar radius of the SPB.

The governing equations for the shape of the ZPB in terms of its natural shape and mass are given in equation 5, 6 and 7 (Mladenov & Oprea, 2009). This equation describes the angular variation (θ) of the balloon's shape, meridional stress function (m), radius function (r) and height function(z) with respect to its path s.

$$\frac{d\theta}{ds}=-\Sigma\rho rm sin\theta+m\tau_b r(z+a)$$

where, $\left[\Sigma=\frac{w_d}{b_d}\left(\frac{b_d}{L}\right)^3, m=\frac{1}{\sigma_m\rho}, \tau_b=\frac{b}{b_d}\right]$

$$\frac{dm}{ds}=-\Sigma\rho rm^2 cos\theta$$

$$\frac{dr}{ds}=-sin\theta$$

$$\frac{dz}{ds}=cos\theta \tag{3}$$

with initial conditions,

$$\theta(0)=-\theta_0, \quad m(0)=2\pi cos\theta_0, \quad r(0)=0, \quad z(0)=0 \tag{4}$$

and boundary conditions,

$$\theta(l)=\pm\frac{\pi}{2}, \quad r(l)=0 \tag{5}$$

where

w_d is the weight density of the balloon,

σ_m is the meridian stress,

τ_b is 1 at float altitude,

l is the balloon's meridian curve's length (during the rise to float, this remains constant) (Mladenov & Oprea, 2009). These equations are used along with the previously described float altitude and payload scenario to construct the shape of the smooth ZPB, as shown in Fig. 1.

In practice, it is often more convenient to construct the surface using a set of pie-shaped panels, known as gores, rather than a continuous smooth curve as shown in Fig. 2. The presence of the gores can also provide structural rigidity to the balloons. For the part of the study that analyzes the effect of the gores on the aerodynamic performance of the balloons as compared to the smooth geometries, only the ZPB is studied. It is expected that the general aerodynamic effect of gores on both types of balloons would be identical. For a pumpkin-shaped SPB, the Taylor curve is generally employed to define the outer curve of the gore; however, for a natural-shaped ZPB, the gore outer curve is approximated similarly to that of the smooth ZPB. The difference in the volume between smooth and gored ZPB was found to be negligible. Each

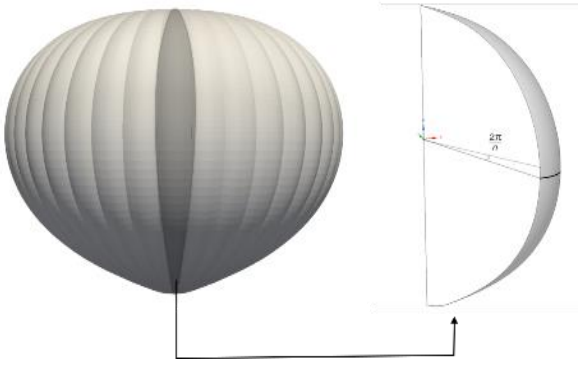

Fig. 2 Gore geometry used for ZPB

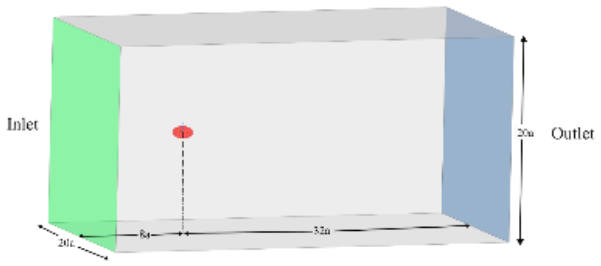

Fig. 3 Computational domain for SPB, a is the length of the equatorial radius

gore has a constant radius and subtends an angle of θ = 2π/*N* at the equatorial plane, where N is the total number of gores. The choice of the number of gores is determined by the desired balance between minimizing surface area and maintaining a smooth outer shape. A higher number of gores will result in a smoother outer shape but will also increase the surface area of the balloon, thereby increasing its weight and material cost.

Boundary conditions play a crucial role in numerical fluid simulations of external flows. The choice of boundary conditions can greatly influence the accuracy and stability of the simulation, and proper consideration must be given to their selection. In this study, converged results of Reynolds-Averaged Navier-Stokes (RANS) simulation were used to initialize the flow over the balloon in the unsteady LES setting. Inlet velocity and pressure outlet boundary conditions were applied. A constant velocity was specified at the inlet, while a freestream pressure boundary condition with a relative pressure value of zero was applied at the outlet. This effectively represents atmospheric pressure at the outlet. Additionally, no-slip boundary conditions were imposed at the balloon walls. 2.5% turbulent intensity at the inlet provided the scope to calculate other turbulent parameters like turbulent kinetic energy(κ), dissipation rate (ϵ), specific dissipation rate (ω) and turbulent viscosity (ν_{sgs}). Once the RANS simulation was converged, the resulting velocity, pressure and turbulence parameters field was used to initialize the LES simulation. The LES simulation then used a more detailed turbulence model to capture the large-scale turbulent structures and the effects of the smaller-scale turbulence on the flow dynamics.

3.3 Mesh Details and Solver Description

The mesh represents the computational domain, and its quality and resolution directly affect the accuracy and stability of the simulation. In this study, ANSYS Fluent mesher was used to generate a mesh for a high-resolution LES simulation for a computational domain of $40a \times 20a \times 20a$ as shown in Fig. 3. The ANSYS Fluent mesher offers a range of meshing techniques, including mosaic meshing, which was used in this study, shown in Fig. 4 Mosaic meshing is a highly flexible and automated meshing technique that allows the user to generate a mesh with a mix of different cell types, including polyhedral, hexahedral, and prism layers. The mesh generated using the mosaic meshing technique was refined near the walls to capture the near-wall turbulence and to resolve the turbulent kinetic energy of more than 80%. The first cell height near the balloon was determined using a y+ value of 1. The mesh parameters such as the maximum non-orthogonality angle of 55.45^o, the maximum aspect ratio of 40.18 and the maximum skewness of 2.01 ensured the quality of the generated mesh for the base case of the smooth SPB. The SPB mesh comprises 1,056,172 nodes, featuring a boundary layer with 15 layers and a growth rate of 1.2, providing a detailed resolution of the flow field around the balloon. It is important to note that the mesh quality and resolution must be carefully monitored to ensure that the simulation results are accurate and stable. This is particularly important for high-resolution LES simulations, where a high-quality mesh is critical for capturing complex flow behavior. By using mosaic meshing with a combination of different cell types and performing a mesh sensitivity analysis, the ANSYS Fluent mesher allows the user to generate a high-resolution mesh that accurately captures the turbulent kinetic energy and provides stable and accurate simulation results.

In the present study, the OpenFOAM open-source code was used for the simulation of the external aerodynamics of the SPB and ZPB. The solver used for the pressure-velocity coupling was the PISO (Pressure Implicit with Splitting of Operators) algorithm, which is a widely used solver in OpenFOAM for incompressible

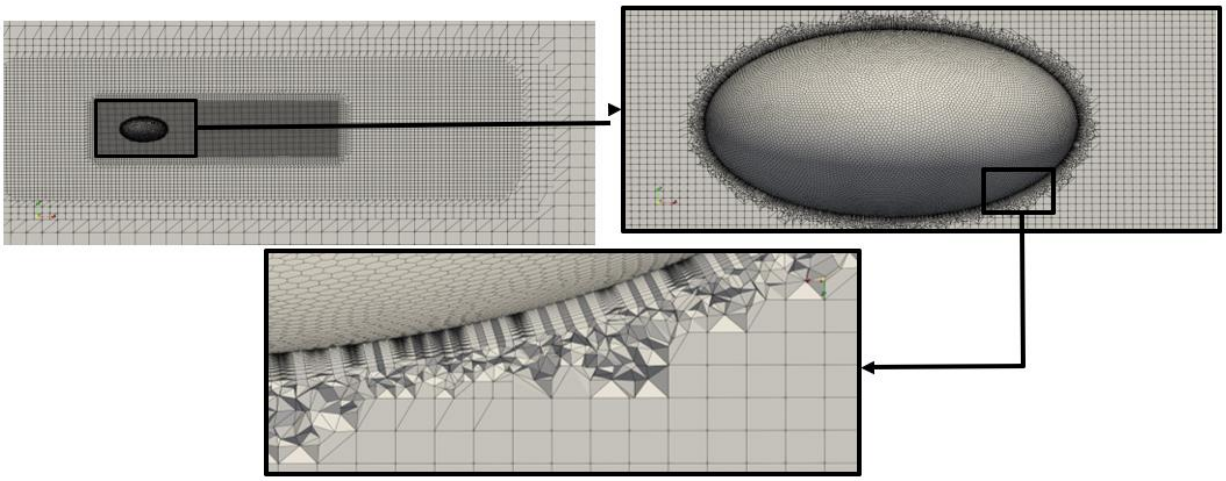

Fig. 4 Mesh configurations for SPB

flow simulations. The solver employs the backward time discretization scheme, which is second-order accurate, for the time integration of the Navier-Stokes equations. The spatial discretization of the momentum equations was performed using the finite volume method, and the divergence of the velocity was discretized using the second-order accurate, Gauss linear scheme. The simulation uses a variable time step fulfilling the CFL= 0.5 criterion, ensuring enough time scale resolution.

4. RESULTS AND DISCUSSION

Convergence is a critical aspect of LES, as it determines the accuracy and reliability of the results. One common measure of convergence in LES simulations is the convergence of the aerodynamic performance measures (i.e C_d in this case) over time. Convergence is typically achieved when these statistical measures converge to a steady-state or quasi-steady-state solution. In the present study, for the SPB simulation, a steady-state solution is achieved in as little as 600 seconds, while the ZPB case takes significantly longer due to greater fluctuations in C_d over time. This difference in convergence time is attributed to the difference in aerodynamic characteristics of the two balloon types, with the more aerodynamic shape of the SPB leading to reduced drag and faster convergence to a steady-state solution.

4.1 Validation of LES Methodology

The LES simulations were conducted using the open-source software OpenFOAM. To validate the methodology used for the analysis of the stratospheric balloons, a sphere was first modeled, and the results were compared to the widely available literature on the subject. The sphere was modeled as a three-dimensional solid object with a diameter of 30 m, in order to have comparable geometry to the balloons. Just as in the case of the balloon analysis, the fluid was assumed to be incompressible and Newtonian, with a density of 0.089 kg/m^3 and kinematic viscosity of $1.61E-4\ m^2s^{-2}$, to represent the flight altitude of 20,000 m. The inlet velocity was set based on the Reynolds number under investigation. For example, an inlet velocity of 0.644 m/s under the previously described fluid conditions corresponds to a Reynolds number of $1.2E5$. The Reynolds number varied from 4E4 to 6E5 by changing the velocity while keeping the sphere diameter and fluid properties constant. The C_d was calculated using the formula in equation 8. In order to validate the LES results, the obtained solution was compared with the correlated drag coefficient of the sphere from the literature (Almedeij, 2008; Morrison, 2013).

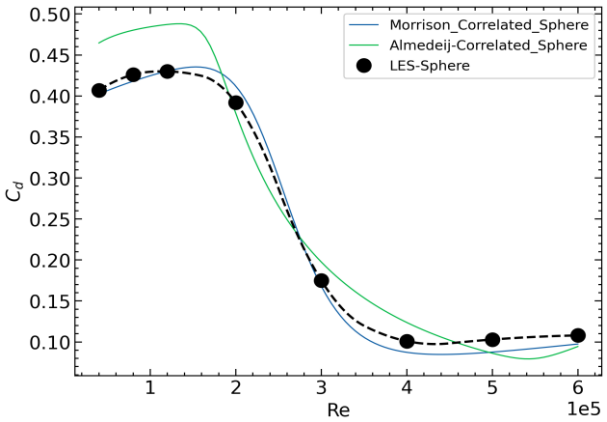

Fig. 5 Comparison of results of the LES simulations to the literature for a sphere and a range of Reynolds numbers (Almedeij, 2008; Morrison, 2013)

$$C_d = \frac{8F_d}{\rho U^2 \pi d^2} \tag{6}$$

where C_d is the drag coefficient, F_d is the drag force, ρ is the fluid density, U is the free-stream velocity, and d is the sphere diameter.

The results of the LES simulations were found to be in good agreement with the data found in the literature over the range of Reynolds numbers considered, as seen in Fig. 5. The range studied included the critical "drag crisis" region of the sphere. The drag coefficient decreased with the increasing Reynolds number. The comparison with the data from the literature confirmed the validity of the simulations and demonstrated the potential of this model for studying fluid flow around stratospheric balloons.

4.2 Drag Analysis of SPB and ZPB

The aerodynamic performance analysis of smooth shapes approximating SPB and ZPB is conducted. The simulation was performed until a steady-state solution was observed, as indicated by the C_d signal. The mean value was then calculated, as presented in Fig. 6. The two types of balloons both differ in their shape and construction, as

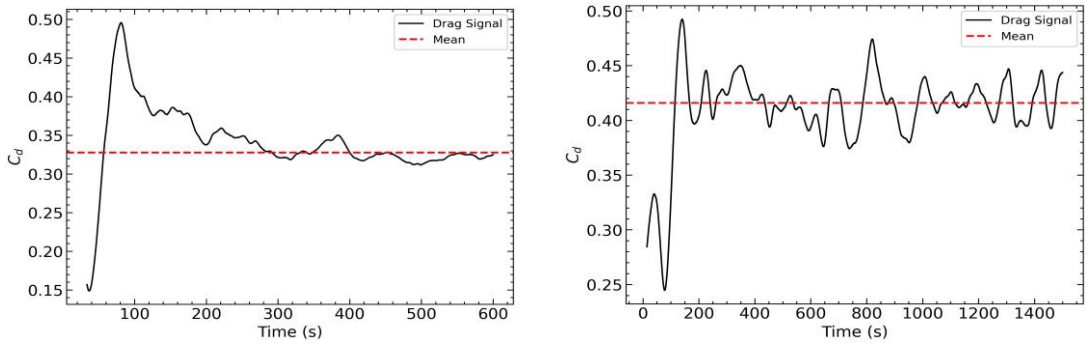

(a) SPB (b) ZPB

Fig. 6 The trace of the Cd during a simulation showing convergence around the mean for Re=1.2E5

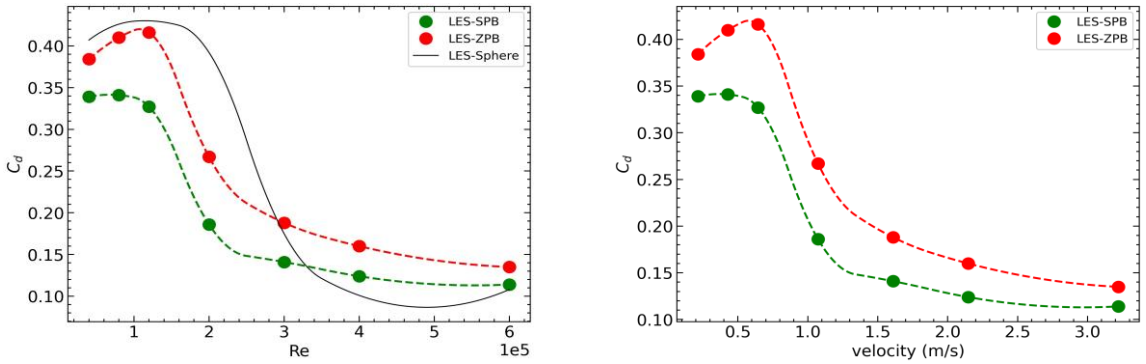

(a) C_d *vs Re* (b) C_d *vs forward airspeed*(m/s)

Fig. 7 Plot for comparison between SPB, ZPB and sphere at 20,000 m

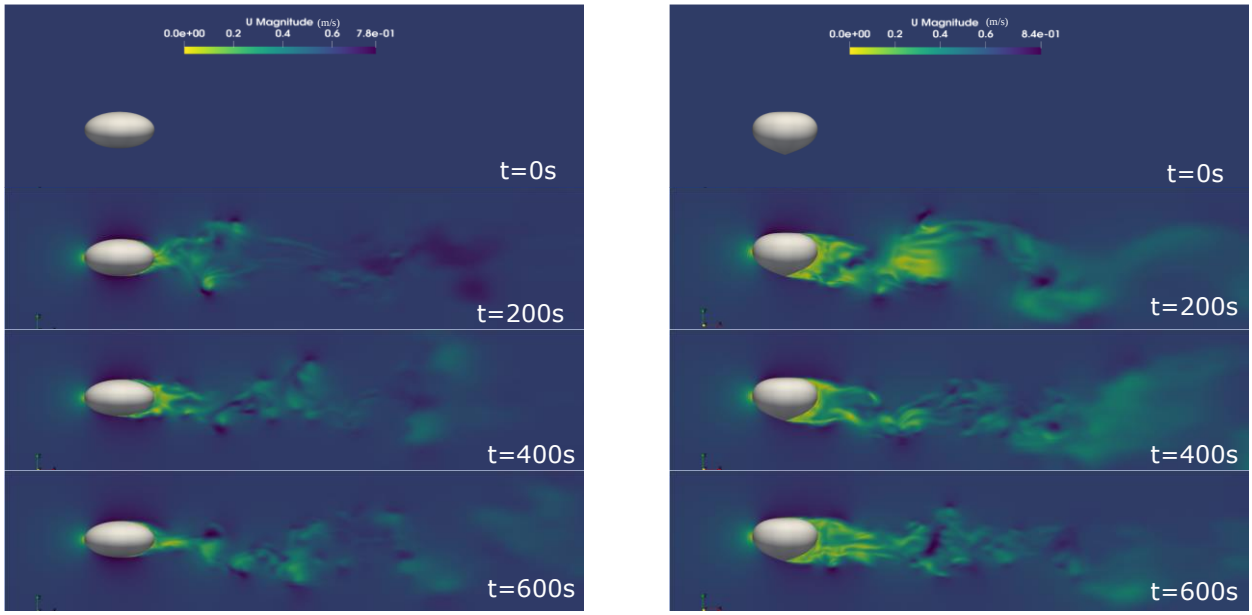

Fig. 8 Sequential time-steps of the velocity around the balloons for Re=1.2E5 (Side view)

well as in their aerodynamic properties. The drag analysis of these two types of balloons is shown in Fig. 7, where it was found that the C_d of both the SPB and ZPB were slightly lower than that of a sphere for Reynolds numbers below 3E5, which occurs midway through the sphere's drag crisis. At higher Reynolds numbers, however, both balloon shapes had a slightly higher drag coefficient. The balloon shapes also experienced a drag crisis, but it was found that this occurred in slightly lower Reynolds numbers than for that of a sphere. The SPB was found to have a lower C_d at all Reynolds numbers when compared to the ZPB.

Flow separation occurs when the airflow around an object becomes unstable due to adverse pressure gradient and separates from the surface of the object. This can result in increased drag, which can be detrimental to the aerodynamic performance of the balloon. As shown in Fig. 8, the velocity contours highlight the wake regions behind both the SPB and the ZPB. The ZPB exhibits a larger wake, indicating significant flow separation and turbulence at the rear of the balloon. This increased wake size correlates with higher drag, negatively impacting its aerodynamic efficiency. In contrast, the SPB shows a narrower and shorter wake region, suggesting that its streamlined design effectively delays flow separation and reduces the associated drag. The more compact wake behind the SPB demonstrates a smoother airflow detachment, which contributes to its superior aerodynamic performance compared to the ZPB.

4.3 Gore Sensitivity Study

The analysis in previous section analyzed the effect of the smooth shapes of the balloons on aerodynamic drag without accounting for the surface geometry as a result of the gores. A sensitivity study was conducted on the number of gores (N) used in the construction of the ZPB to investigate its effect on the balloon's performance. The number of gores varied between N = 30, 40, and 50 while keeping the radius of the gore constant. It should be noted that the study on higher numbers of gores was limited due

Table 2 Flow separation point and drag coefficient for ZPB with gores

	N=30	N=40	N=50
Flow separation angle	77^o	56^o	44^o
C_d	0.328	0.270	0.223

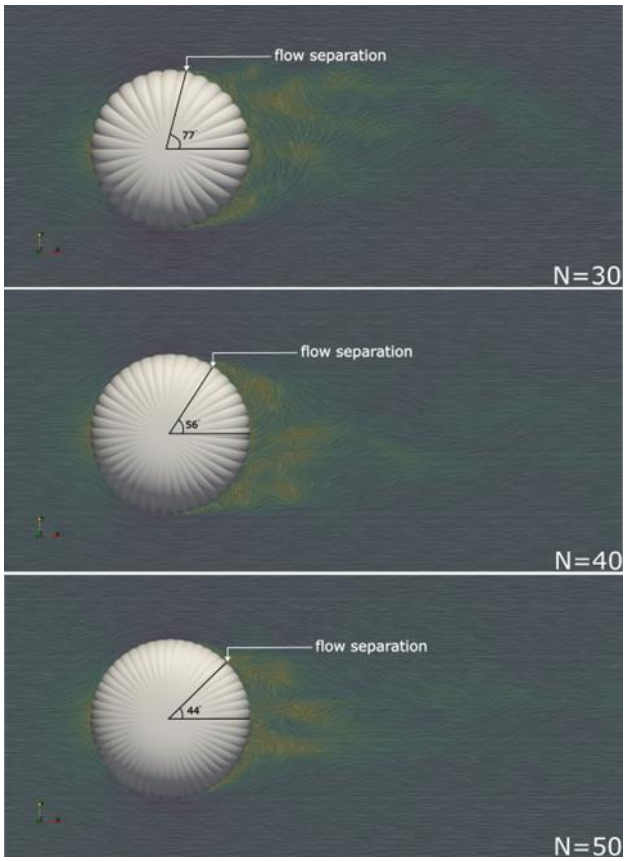

Fig. 9 Flow separation point at the upper-half (Top view) of the ZPB streamline plot for a varied number of gores

to computational constraints, as using a larger number of gores resulted in extremely small mesh sizes. The sensitivity study was conducted using the same LES setup as the previous simulations, at a Reynolds number of 6E5 for the ZPB case.

The results of the sensitivity study indicated that the number of gores had a significant impact on the aerodynamic performance of the ZPB. At a low number of gores, the C_d is relatively high compared to the smooth case. This value decreases with an increase in the number of gores, presumably asymptotically until the smooth case, which is equivalent to N = ∞. This result likely occurs as a result of the earlier flow separation experienced at a low number of gores, due to comparatively large changes in the curvature near the balloon surface. The flow separation angle for N=30 was determined to be at 77^o, at 56^o for N=40 and at 44^o for N=50 as seen in Fig. 9. This figure highlights how the flow behind the ZPB becomes more streamlined as the number of gores increases. The results show that at lower gore counts, the wake is wider and more turbulent, contributing to increased drag. In contrast, as the gore count rises, the wake narrows, indicating more efficient flow reattachment and reduced turbulence.

While certain geometric assumptions were made in modeling the case with gores, it is quite possible to have slightly different configurations for the same number of gores, depending on construction and design. Thus, these values are meant to be more qualitatively informative as opposed to broadly applicable, due to the variant nature of the design. There is evidence that NASA has operated balloons ranging from 48 to 180 gores, and Raven Industries have tested balloons between 48 and 290 gores (Smith & Rainwater, 2004; Cathey Jr, 2009; Cathey & Fairbrother, 2013). Thus, using an interpolated C_d slightly above the smooth case solution depending on the exact number of gores under test could be a viable approach in practical applications. Further research into the nuances of geometric construction, gore design, and surface effects relative to the smooth shape are encouraged in order to develop relationships for this effect.

5. CONCLUSIONS

The aerodynamic drag properties of stratospheric balloons are important in order to accurately model balloon trajectory predictions, station-keeping simulations, as well as engineering design for horizontal propulsion-based balloon systems This study used computational LES methods to find that the drag for both superpressure balloons and zero pressure balloons differed slightly from that of a sphere when their outer shapes were modeled as smooth geometries.

Some of the key findings of the present work are as follows:

1. The simulations displayed qualitatively similar characteristics to a sphere across the Reynolds number range, including the drag crisis effect at transition.
2. The drag crisis for balloons occurs at an earlier Reynolds number when compared to a sphere.
3. It was found that the SPB had a more streamlined shape compared to the ZPB for all Reynolds numbers investigated.
4. The effect of modeling the balloon gores was investigated, showing a decrease in drag coefficient as the number of gores increased. For instance, increasing the number of gores from 30 to 50 resulted in a 32% reduction in drag.

CONFLICT OF INTEREST

The authors declare no conflicts to disclose.

AUTHORS CONTRIBUTION

Binayak Lohani: Methodology (lead), Investigation (equal), Data curation (lead), Validation (lead). **Craig Mascarenhas**: Supervision (lead), Conceptualization (lead)

REFERENCES

Aaron, K., Heun, M., & Nock, K. (2002). A method for balloon trajectory control. *Advances in Space Research*, *30*(5), 1227–1232. https://doi.org/10.1016/S0273-1177(02)00526-4

Akhlaghi, M., Asadbeigi, M., & Ghafoorian, F. (2023). on Novel CFD and DMST dual method parametric study and optimization of a Darrieus vertical axis wind turbine. *Journal of Applied Fluid Mechanics*, 17(1), 205-218. https://doi.org/10.47176/jafm.17.1.1985

Almedeij, J. (2008). Drag coefficient of flow around a sphere: Matching asymptotically the wide trend. *Powder Technology*, *186*, 218–223. https://doi.org/10.1016/j.powtec.2007.12.006.

Cathey Jr, H. (2009). The nasa super pressure balloon–a path to flight. *Advances in Space Research*, *44*(1), 23–38. https://doi.org/10.1016/j.asr.2009.02.013

Cathey, H. M., & Fairbrother, D. A. (2013). *The 2012 nasa˜ 532,200 m3 super pressure balloon test flight.* AIAA Balloon Systems (BAL) Conference (p. 1269).

Dai, Q., Fang, X., Li, X. & Tian, L. (2012). Performance simulation of high altitude scientific balloons. *Advances in Space Research*, *49*(6), 1045–1052. https://doi.org/10.1016/j.asr.2011.12.026

Du, H., Li, J., Zhu, W. Qu, Z., Zhang, L., & Lv, M. (2019a). Flight performance simulation and station-keeping endurance analysis for stratospheric super-pressure balloon in real wind field. *Aerospace Science and Technology*, *86*, 1–10. https://doi.org/10.1016/j.ast.2019.01.001

Du, H., Lv, M., Li, J. Zhu, W., Zhang, L., & Wu, Y. (2019b). Station-keeping performance analysis for high altitude balloon with altitude control system. *Aerospace Science and Technology*, *92*, 644–652. https://doi.org/10.1016/j.ast.2019.06.035

Dykema, J., Keith, D., Anderson, J. & Weisenstein, D. (2014). Stratospheric controlled perturbation experiment: A small-scale experiment to improve understanding of the risks of solar geoengineering. *Philosophical transactions. Series A, Mathematical, Physical, and Engineering Sciences*, *372*. https://doi.org/10.1098/rsta.2014.0059.

Farley, R. (2005). Balloonascent: 3-d simulation tool for the ascent and float of high-altitude balloons. *AIAA 5th ATIO and16th Lighter-Than-Air Sys Tech. and Balloon Systems Conferences* (p. 7412). https://doi.org/10.2514/6.2005-7412

Fesen, R., & Brown, Y. (2015). A method for establishing a long duration, stratospheric platform for astronomical research. *Experimental Astronomy*, *39*, 475–493. https://doi.org/10.1007/s10686-015-9459-9

Garde, G. (2005). *Comparison of two balloon flight simulation programs*. AIAA 5th ATIO and16th Lighter-Than-Air Sys Tech. and Balloon Systems Conferences (p. 7413). https://doi.org/10.2514/6.2005-7413

Ghafoorian, F., Mirmotahari, S. R., Wan, H. (2024). Numerical study on aerodynamic performance improvement and efficiency enhancement of the savonius vertical axis wind turbine with semi-directional airfoil guide vane. *Ocean Engineering*, *307*. https://doi.org/10.1016/j.oceaneng.2024.118186

Givi, P. (1989). Model-free simulations of turbulent reactive flows. *Progress in Energy and Combustion Science*, *15*(1), 1–107. URL: https://doi.org/10.1016/0360-1285(89)90006-3.

Jewtoukoff, V., Plougonven, R., Hertzog, A. Snyder, C., & Romine, G. (2016). On the prediction of stratospheric balloon trajectories: improving winds with mesoscale simulations. *Journal of Atmospheric and Oceanic Technology*, *33*(8), 1629–1647. https://doi.org/10.1175/JTECH-D-15-0110.1

Kahyan, Ö. (2020). Station keeping of wind driven stratospheric balloon via propulsion unit. *Journal of Engineering Sciences and Design*, 8(1), 252-261. https://doi.org/10.21923/jesd.397265

Lesieur, M., & Metais, O. (1996). New trends in large-eddy simulations of turbulence. *Annual Review of Fluid Mechanics*, *28*(1),45–82. https://doi.org/10.1146/annurev.fl.28.010196.000401

Li, J., Liao, J., Liao, Y. Du, H., Luo, S., Zhu, W., & Lv, M. (2018). An approach for estimating perpetual endurance of the stratospheric solar-powered platform. *Aerospace Science And Technology*, *79*, 118–130. https://doi.org/10.1016/j.ast.2018.05.035

Liu, Y., Xu, Z., Du, H. & Lv, M. (2022). Increased utilization of real wind fields to improve station-keeping performance of stratospheric balloon. *Aerospace Science and Technology*, *122*, 107399. https://doi.org/10.1016/j.ast.2022.107399

Lohani, B., Foran, D., Mohammadian, A., & Nistor, I. (2022). Numerical model of a tidal current acceleration structure. *Journal of Renewable and Sustainable Energy*, *14*(5), 054502. URL: https://doi.org/10.1063/5.0104471.

Menon, S., Yeung, P., & Kim, W. (1996). Effect of subgrid models on the computed interscale energy transfer in isotropic turbulence. *Computers & Fluids*, *25*(2), 165–180. https://doi.org/10.1016/0045-7930(95)00036-4.

Miller, G., Stoia, T., Harmala, D. & Atreya, S. (2005). *Operational capability of high altitude solar powered airships.* AIAA 5th ATIO and16th Lighter-Than-Air Sys Tech. and Balloon Systems Conferences (p. 7487). https://doi.org/10.2514/6.2005-7487

Mladenov, I., & Oprea, J. (2009). Balloons, domes and geometry. *J. Geom. Symmetry Phys.*, *15*, 53–88.

https://doi.org/10.7546/jgsp-15-2009-53-88.

Moin, P., & Kim, J. (1982). Numerical investigation of turbulent channel flow. *Journal of Fluid Mechanics*, *118*, 341–377. https://doi.org/10.1017/S0022112082001116.

Morrison, F. A. (2013). *An introduction to fluid mechanics*. (Cambridge University Press, New York, 2013). This correlation appears in Figure 8.13 on page 625., 186. https://doi.org/10.1017/CBO9781139047463

Musso, I., Cardillo, A., Cosentino, O. & Memmo, A. (2004). A balloon trajectory prediction system. *Advances in Space Research*, *33*(10), 1722–1726. https://doi.org/10.1016/j.asr.2003.07.044

Palumbo, R., Russo, M., Filippone, E. & Corraro, F. (2007). *Achab: Analysis code for high-altitude balloons*. AIAA Atmospheric Flight Mechanics Conference and Exhibit (p. 6642). https://doi.org/10.2514/6.2007-6642

Ramesh, S. S., Ma, J., Lim, K. M. Lee, H P., & Khoo, B C. (2018). Numerical evaluation of station-keeping strategies for stratospheric balloons. *Aerospace Science and Technology*, *80*, 288–300. https://doi.org/10.1016/j.ast.2018.07.010

Raque, S., & Robbins, E. (2012). *Recent developments in the sinbad balloon vertical performance model*. 32nd Aerospace Sciences Meeting and Exhibit. URL: https://arc.aiaa.org/doi/abs/10.2514/6.1994-517.

Saleh, S., & He, W. (2017). Ascending performance analysis for high altitude zero pressure balloon. *Advances in Space Research*, *59*(8), 2158–2172. https://doi.org/10.1016/j.asr.2017.01.040

Schur, W. (2002). The design process for a pumpkin balloon: structural synthesis, structural analysis, and analytical assessment of some critical design issues. *Advances in Space Research*, *30*(5), 1193–1198. https://doi.org/10.1016/S0273-1177(02)00532-X

Smith, I. (2002). The nasa balloon program: an overview. *Advances in Space Research*, *30*(5), 1087–1094. https://doi.org/10.1016/S0273-1177(02)00518-5.

Smith, M., & Rainwater, E. (2004). Optimum designs for superpressure balloons. *Advances in Space Research*, *33*(10), 1688–1693. https://doi.org/10.1016/j.asr.2003.07.042

Sóbester, A., Czerski, H., Zapponi, N.& Castro, I. (2014). High-altitude gas balloon trajectory prediction: a monte carlo model. *AIAA Journal*, *52*(4), 832–842. https://doi.org/10.2514/1.J052900

Sun, Q., Lim, K.-M., Lee, & Khoo, B. (2015). *Air drag on a stratospheric balloon in tropical regions.* Academic High Altitude Conference. Iowa State University Digital Press volume 2015. https://doi.org/10.31274/ahac.5572

Tang, J., Pu, S., Yu, P. Xie, W., Li, Y., & Hu, B. (2022). Research on trajectory prediction of a high-altitude zero-pressure balloon system to assist rapid recovery. *Aerospace*, *9*(10), 622. https://doi.org/10.3390/aerospace9100622

Tian, Y., Lin, G., Guo, J. (2023). Drag crisis analysis of a high-altitude balloon in critical transition. *Aerospace Science and Technology*, *109*. https://doi.org/10.1016/j.ast.2023.108396

van Wynsberghe, E., & Turak, A. (2016). Station-keeping of a high-altitude balloon with electric propulsion and wireless power transmission: A concept study. *Acta Astronautica*, *128*, 616–627. https://doi.org/10.1016/j.actaastro.2016.08.017